Large asymmetric polar scarps on Planum Australe, Mars: Characterization and evolution

Cyril Grima, F. Costard, Wlodek Kofman, Bertrand Saint-Bézar, Anthony Servain, Frédérique Rémy, Jérémie Mouginot, Alain Herique, Roberto Seu

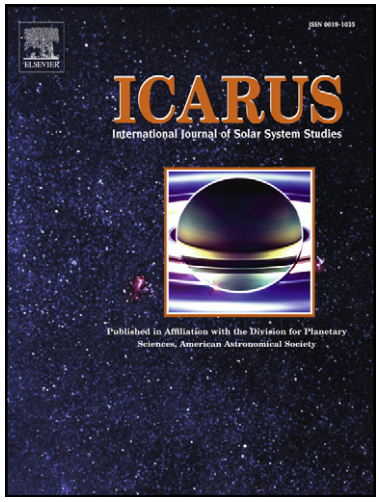

Large asymmetric polar scarps on Planum Australe, Mars: Characterization and evolution

Cyril Grima, François Costard, Wlodek Kofman, Bertrand Saint-Bézar, Anthony Servain, Frédérique Rémy, Jérémie Mouginot, Alain Herique, Roberto Seu

PII: S0019-1035(10)00485-9
DOI: 10.1016/j.icarus.2010.12.017
Reference: YICAR 9668

To appear in: *Icarus*

Received Date: 12 April 2010
Revised Date: 17 December 2010
Accepted Date: 18 December 2010

Please cite this article as: Grima, C., Costard, F., Kofman, W., Saint-Bézar, B., Servain, A., Rémy, F., Mouginot, J., Herique, A., Seu, R., Large asymmetric polar scarps on Planum Australe, Mars: Characterization and evolution, *Icarus* (2010), doi: 10.1016/j.icarus.2010.12.017

Large asymmetric polar scarps on Planum Australe, Mars: Characterization and evolution

Cyril Grima[1]	(email) cyril.grima@obs.ujf-grenoble.fr	(tel.) +33 4 76 63 52 81
François Costard[2]	(email) francois.costard@u-psud.fr	(tel.) +33 1 69 15 49 10
Wlodek Kofman[1]	(email) wlodek.kofman@obs.ujf-grenoble.fr	(tel.) +33 4 76 51 41 47
Bertrand Saint-Bézar[2]	(email) bertrand.saint-bezar@u-psud.fr	(tel.) +33 1 69 15 67 93
Anthony Servain[1]	(email) berkuts37@hotmail.fr	
Frédérique Rémy[3]	(email) remy.omp@free.fr	(tel.) +33 5 61 33 29 58
Jérémie Mouginot[4]	(email) jmougino@uci.edu	(tel.) 281 486 2146
Alain Herique[1]	(email) alain.herique@obs.ujf-grenoble.fr	(tel.) +33 4 76 51 41 73
Roberto Seu[5]	(email) roberto.seu@uniroma1.it	(tel.) +39 06 4458 5943

[1]Laboratoire de Planétologie de Grenoble (CNRS/UJF, UMR5109), 38041 Grenoble Cedex, France
[2]Interactions et Dynamique des Environnements de Surface, (CNRS/UPS, UMR8148), Orsay, France
[3]Laboratoire Etudes en Géophysique et Océanographie Spatiale (CNES/CNRS/UPS), Toulouse, France
[4]University of California, Department of Earth System Science, Irvine, CA 92697-3100 USA
[5]Dipartimento InfoCom, Università di Roma "La Sapienza", Rome, Italy

Pages = 33 Figures = 12 Tables = 1

Running Head: Large asymmetric polar scarps on Planum Australe

Corresponding author:

Cyril Grima

Laboratoire de Planétologie de Grenoble - BP 53

38041 Grenoble Cedex 9 - France

(tel.) +33 4 76 63 52 81

(fax.) +33 4 76 51 41 46

cyril.grima@obs.ujf-grenoble.fr

Abstract

Numerous scarps with similar characteristics have been observed in the polar layered deposits of Planum Australe, Mars. They are referred to as LAPSs (for Large Asymmetric Polar Scarps) because of their typical cross-section featuring a trough between a straight slope on one side with outcrops of layered deposits and a convex slope on the other side without any outcrops. These LAPSs are restricted to the outlying region of Ultimi Lobe. Topographic data, optical images, and subsurface radar observations have been analyzed and compared to produce a complete morphologic and stratigraphic description of these scarps. In all, 167 LAPS-like features have been identified. All have similar dimensions and characteristics and appear to be deep depressions in the ice. The polar deposits have an average thickness of 1 km in this region and the LAPS depressions commonly reach half of that thickness. Subsurface data indicate that the depressions could reach bedrock at certain locations. Many surface features of the polar deposits of Mars are considered to be consequences of depositional and/or erosion processes. We propose a mechanical failure of the ice for the LAPSs origin, given the striking similarities in shape and size they show with rollover anticlines above listric faults commonly observed as a crustal extension mode on Earth. This tectonic scenario would imply a substantial outward sliding of the polar deposits in the region of Ultimi Lobe and a low basal shear stress. No information is available to determine whether such a system could be active at present. Confirmation of the "mechanical failure" hypothesis of these LAPSs on Mars is of major importance as it could be a macro-expression of fundamental differences between ice-sheet behavior under Martian and Terrestrial conditions.

Keywords: Mars, polar geology; Mars, polar caps; Ices; Radar observations; Tectonics

1. Introduction

The south and north polar plateaus of Mars - respectively Planum Australe and Planum Boreum - are the only known examples of extraterrestrial ice-sheets comparable to those of the Earth. Many striking similarities with the Earth's ice-sheets exist. For instance, the volumes of both Planum Australe and Planum Boreum (respectively ~1.6 $x10^6$ km^3 and ~1.1 $x10^6$ km^3) are of the same order as that of the Greenland ice sheet (~2.6 $x10^6$ km^3), with similar average thicknesses of about 1000 to 1500 m (Plaut et al., 2007; Smith et al., 2001; Weidich, 1995). Moreover, water ice is the major ice-sheet component on both Earth and Mars, with an average impurity fraction that is likely less than 10% for Planum Australe (Plaut et al., 2007) and close to 5% for Planum Boreum (Grima et al., 2009). When the mass-balance is positive, the growth process of ice sheets on both planets is driven by the deposition of isochronous layers (known on Mars as polar layered deposits, PLD). Their impurity contents vary with the time of deposition (Cutts and Lewis, 1982; Thomas et al., 1992). Furthermore, the ice of the Earth's ice sheets is crystallized in the hexagonal system (ice-Ih). Although cubic ice (Ice-Ic) could form under Martian conditions by vapor deposition on the surface, it would be metastable (Gooding, 1988). Given the annual rise of surface temperature above the Ic/Ih irreversible transition (~150 K), the Martian ice sheets are likely exclusively composed of stable ice-Ih as on Earth. And finally, the evolution of the ice sheets on a geological time-scale is mainly driven by Milankovitch orbital cycles (obliquity, eccentricity, and precession variations) leading to planetary climate forcing (Hays et al., 1976; Head et al., 2003), as on Earth.

Nevertheless, the polar environment on Mars is different than on Earth. For instance, temperatures in Martian polar regions can be as low as 150 K in both hemispheres (Lewis et al., 1999), while the average surface pressure is 0.008 bars with seasonal variations of ± 20% (Clifford et al., 2000) and gravity is 0.38 times less than on Earth. Furthermore, the base elevations of the two Martian polar plateaus differ by around 6000 m, far more than on Earth. On Mars, the geothermal heat flow that largely determines the basal temperature of a glacier is estimated to be in the range of 15 to 45 mW m^{-2} (e.g. McGovern et al., 2004; Nimmo and Stevenson, 2000; Reese et al., 1998), lower than the value of ~65 mW m^{-2} for the Earth's continents (Pollack et al., 1993). Consequently, the surface mass balance of the Earth's ice sheets is mainly determined by melting of snow and ice, whereas condensation and sublimation are the dominant processes on Mars (Rognon et al., 2007). Orbital parameters vary with a comparable timescale on Mars and Earth, but with greater amplitudes on Mars. Over the past 10 Myr, Martian obliquity has exceeded 45° and the eccentricity of the orbit has reached maximums twice that of the Earth's (Laskar et al., 2002; Ward, 1992). Taking all these similarities and dissimilarities into account, Mars can be considered as a full-scale laboratory for the study of the behavior of an Earth-like ice-sheet system over extended conditions. Consequently, the peculiarities observed on the Martian polar plateaus can help us improve our understanding of the Earth's ice-sheet system in general and make the first steps toward meaningful comparative planetology in polar science.

With this in mind, this paper provides a geomorphologic description of polar scarps frequently observed in the region of Ultimi Lobe (UL), Planum Australe (see Fig. 1). Despite their km-size and typical asymmetric profile that will be described, equivalent formations have never been reported to date on polar glaciers on Earth. Because of their particular shape, we call these formations LAPSs (for Large Asymmetric Polar Scarps). Until now, only a few studies have

reported such LAPSs on Viking images (Howard, 2000; Thomas and Weitz, 1989), attributing them to an eolian origin. Here LAPSs are described by coupling optical images, surface topography, and radar sounding from recent datasets. This multi-instrumental approach makes it possible to establish profiles of the surface and subsurface of the LAPSs. A LAPS inventory was undertaken and 167 corresponding formations were identified across UL, providing geomorphologic elements to identify and discuss different formation processes for LAPSs. Most of the observations appear to be consistent with a mechanical failure of the ice, analogous to a "listric fault/rollover" system. This tectonic process will be discussed along with certain direct implications.

2. Regional context

Planum Australe overlies heavily cratered highlands that are reported to be Noachian and Hesperian in age (Tanaka and Scott, 1987). The middle-Hesperian Dorsa Argentae Formation (DAF) is thought to be the youngest surrounding terrain ~~of Planum Australe~~. The Planum Australe mound accumulated during the late Amazonian period (Kolb and Tanaka, 2001) and presently has a maximum thickness of 3700 m (Plaut et al., 2007). Cratering records estimate the plateau's surface to be as old as 10 to 100 My (Herkenhoff and Plaut, 2000; Koutnik et al., 2002). Signatures of the former extent of the ice sheet have been observed in the DAF where esker-like ridges could be the consequence of past basal-melting (Head and Pratt, 2001; Kargel and Strom, 1992; Milkovich et al., 2002). Present-day conditions on Mars preclude exceeding the melting temperature of water ice, except in cases of substantial geothermal anomalies (Clifford, 1987), not likely to be detected by any in-flight instrument, or in the case of saline water (Renno et al.,

2009 and references therein). UL is an outlying region of Planum Australe, opposite DAF and extending over equivalent latitudes. It is the only part of Planum Australe below 80°S, with latitudes as low as 72°S (Fig. 1). It covers 400,000 km² (i.e. one-third of the entire plateau area). Without this region Planum Australe would be almost perfectly symmetric instead of being offset from the pole. UL seems to have been subjected to a slight outward horizontal motion during recent geological times, revealed by two opposing signatures co-existing along its border. The first is a viscous deformation of the ice, suggested by glacial tongue-like mounds flowing outward in a series of craters dotting the edge of UL (Byrne, 2003). Similar behavior was reported by Head (2001) in the nearby region of Promethei Lingula. The other glacial signature involves brittle processes such as slumping, landsliding and faulting that have also been reported all along the northern border of UL (Byrne, 2003; Murray et al., 2001). These fractures were interpreted as evidence of modest basal sliding of the whole region, seen as a brittle plate.

* Location of Fig. 1 (1.5 column width).

3. Data

Five different data sources were used for this study:

(i) The digital elevation model of the surface acquired by the Mars Orbiter Laser Altimeter (MOLA) (Smith et al., 2001). We used the gridded polar map at 256 pixels/° (~230 m/pixel) with a vertical accuracy of 1 m.

(ii) Visible images from the High Resolution Imaging Science Experiment (HiRISE) with a resolution of 25 to 32 cm/pixel (McEwen et al., 2007). Only a few HiRISE images are available over UL.

(iii) Visible images from the High-Resolution Stereo Camera (HRSC) experiment with a resolution of 10 to 20 m/pixel (Jaumann et al., 2007). Despite a more limited resolution than HiRISE, HRSC were retained because of its high coverage of the UL region.

(iv) Radar subsurface cross-sections (radargrams) of Planum Australe from SHAllow RADar (SHARAD) (Seu et al., 2004). The radar signal (20 MHz) penetrates as deep as ~ 1500 m into water ice materials with 10 × 300 m vertical × along-track resolution. The radar waves are back-scattered by dielectric gradients along the propagation path that are closely related to impurity ~~rate~~ variations in the ice. Thus, SHARAD is able to detect the layers forming Planum Australe. In UL, the detection signal is faint and can suddenly disappear before reappearing tens of kilometres downtrack. This could be due to a low dielectric contrast between isochronous layers. However, the regional density of SHARAD data is high and it was possible to select some radargrams to support morphologic interpretations. Initially, radargrams have a vertical timescale representing the time delay of the echoes. They have been migrated in depth by using a relative dielectric constant of 3.10 as inferred by Grima et al. (2009) for the nearly pure ice of Planum Boreum. Off-nadir surface reflections (clutter) can generate highly delayed echoes that can be confused with subsurface structures. Adaptation of radar simulation developed by Nouvel et al. (2004) allowed us to identified the biggest clutters.

(v) Bedrock elevation as mapped by Plaut et al. (2007) based on the Mars Advanced Radar for Subsurface and Ionosphere Sounding (MARSIS) data (Picardi et al., 2005). Compared to SHARAD, the MARSIS wavelength (1.8 to 5 MHz) provides a lower vertical resolution of ~80 m in the ice. However the signal penetrates deep enough into Planum Australe to be clearly back-

scattered by the bedrock. The vertical uncertainty on the inferred basal topography is assumed to be 200 m (Plaut et al., 2007). It must be emphasized that this bedrock elevation map were obtained by interpolation of a limited-density dataset: the resolution was sufficient to get the basal regional trend but not to detect local anomalies of the bedrock.

4. Morphological description

4.1. Spatial shape and distribution

The first recognizable feature of the LAPSs is their spatial shape. They appear to be arch-shaped, tens of kilometers long, and are distributed over the surface of the ice (Fig. 1). Howard (2000) described this particular signature as a scalloped or a "gull-winged" shape. This criterion enabled us to identify 167 LAPSs over Ultimi Lobe (Fig. 2). This count is not accurate for two reasons: (i) sometimes up to three or more LAPSs are aligned and/or connected, often making it difficult to precisely define how many LAPS there actually are; (ii) the arch-shaped LAPSs can be confused with the rims of shallow-buried craters. To avoid this, we do not consider scarps that are obviously linked to a circular structure (an example is shown Fig. 5B). However, since the surface topography is quite disturbed, we cannot rule-out that some less obvious crater-linked formations were counted. The count shows that LAPSs are widespread over Ultimi Lobe. Their "horn-to-horn" width is in the range of 10 to 20 km, while some can reach 50 km. Most of them are gathered in aligned series. As already observed by Howard (2000), their regular size and close spacing cannot be universally explained by a crater rim origin. This strongly supports the assumption that most of the LAPSs considered in this study are not mainly linked to shallow-

184 buried craters. As shown in Fig. 3, the concave sides of the LAPSs never face the South Pole and
185 the dominant orientation is not towards the equator (i.e. azimuth = 0°). Neither is the orientation
186 constant with respect to longitude. For instance, in a given area, adjacent LAPSs can be almost
187 right-angled (e.g. white arrows in Fig. 2). The regional orientation in the polar stereographic view
188 is also a relevant parameter. Let us define 0° and 90° as the angles for which LAPS concavities
189 face the bottom and the right border of the map respectively. Figure 3 shows this regional
190 orientation in a circular histogram. The whole set of LAPSs appears to be essentially directed
191 towards the same quadrant between 0° and 90°.
192
193 * Location of Fig. 2 (no particular restriction on the size).
194 * Location of Fig. 3 (no particular restriction on the size).
195
196 *4.2. Cross-section*
197
198 The second noteworthy feature is the asymmetric shape of LAPS cross-sections (giving them the
199 second letter of their acronym). They exhibit a trough between a straight slope on one side,
200 comparable to a scarp, facing a gentle convex upward slope on the other side that flattens as it
201 rises. Figure 4 and the cross-sections in Fig. 6 illustrate this profile. The LAPS system forms
202 extremely deep troughs in the ice with respect to the local ice thicknesses. The height of the
203 scarps ranges from 200 m to 700 m with an average value of 400 m. The East part of UL (left
204 side on the map) hosts the highest scarps. The resulting troughs regularly penetrate Planum
205 Australe to half its thickness. In some cases, the trough reaches the top value of the basal
206 elevation estimated by MARSIS. This usually occurs when the trough seems flat and parallel to
207 the bedrock slope, as shown in Fig. 6 for cross-sections 1b-1b'and 3b-3b'. This leads to the

possibility that the bedrock could in some cases become locally exposed. Some LAPSs exhibit a more complex topography on the side of the convex slope (cross-sections 4a-4a'and 4b-4b'). Their curved shape is broken by one or more flat plateaus, more or less horizontal. These LAPSs are essentially located in the heart and in the Eastern part of UL (left side of Fig. 2). Despite these very particular topographies - asymmetric and deep troughs - it is important to emphasize the relative flatness of the system. The slope of the scarps ranges from 2° to 15°, with an average value of 10°. Indeed, the mean horizontal distance between the foot and the top of the straight slope is 3.5 km. Therefore, the horizontal scale of the LAPS system is roughly an order of magnitude larger than the ice thickness. This thinness and flatness are highlighted in Fig. 6 by the inserts that display no vertical exaggeration.

* Location of Fig. 4 (no particular restriction on the size).

4.3. Hillocks

Another feature is regularly (but not systematically) superimposed on the typical cross-section described above i.e. a ridge that can be observed along certain scarp crests (indicated by black arrows in Fig. 6), similar to elongated hillocks. We did not find any relation between the heights of the hillocks and the height of the straight slope or any other distinctive dimensions. The hillock / straight-slope height ratio is usually < 0.2, although around 10 LAPSs, mostly concentrated in the far-east side of UL, have a ratio > 0.5. However, note that the hillocks remain extremely flat, as they are stretched horizontally over 2 to 5 km.

* Location of Fig. 5 (as wide as possible).

* Location of Fig. 6 (as wide as possible).

5. Stratigraphy

The behavior of the internal structure of any geological formation is necessary to understand its origin. Consequently the structure of the PLD beneath the LAPS and information from subsurface radar are essential. However, as noted in section 3, the layers detected by SHARAD in the UL region correspond to faint signals. To support the radar observations, we compared them with visible images from HiRISE and HRSC. These cross-analyses made it possible to draw a partial pattern for the polar layers.

Figure 7 shows two LAPS cross-sections associated with two SHARAD radargrams. HRSC images of the surface along the groundtracks are also shown. The radargram of cross-section 5-5' clearly shows horizontal layers on the straight-slope side (right side of the picture), leading to the hypothesis that the scarp includes outcrops there. On the other side, the layers below the convex slope are curved, parallel to the surface and plunging. Unlike the case on the straight-slope side, no outcrops are expected on the convex slope. On the HRSC image associated with this cross-section, polar layer outcrops can be distinguished as gathered lines of various albedos perpendicular to the ground-track. The change in albedo is due to slope and dust content variations from one layer to another. The cross-section locates these outcrops in an area corresponding exclusively to the straight slope, confirming the radar observation. Conversely, the HRSC image does not show any such signature on the convex slope, consistent with the previous hypothesis that the layers are curved downward and do not outcrop on this side. Cross-section 6-6' shows similar behavior, although the bending of the convex-slope layers is not as clear on the

radargram because of the faint detection signals. However the associated HRSC image reveals that outcrops occur only on the straight slope, implying that the convex-slope layers also plunge downward as supposed.

This asymmetric behavior of the polar layers (outcrops on the straight slope and downward bending below the convex slope) cannot be verified by radar data for the entire set of LAPSs because of the poor layer detection in the UL region as mentioned above. However, visual inspection of available images shows that outcropping on the straight slope only is a common signature of the LAPSs. Figure 8 is an example of a HiRISE image over two successive LAPSs. The asymmetric outcrop is clear for both; however the cross-section path cuts the end of the second LAPS leading to progressive fading of the outcrops.

Finally, it is not possible to comment on the structure just under the LAPS troughs given that no formation is detected by radar. This does not necessarily mean that no reflector is present. It is more likely due to the straight slope, refracting most of the back-wave power offside with respect to the instrument, making underlying features hard to detect. In addition, the recurrent clutter echoes at this location could be strong enough to hide faint signals from the subsurface.

* Location of Fig. 7 (as wide as possible).

* Location of Fig. 8 (as wide as possible).

6. Interpretations

The results of the morphologic description of the LAPS surface and the stratigraphic study are summarized in Fig. 4. The different indicators support that Fig. 4 is a roughly general model for the LAPS morphology. We will now look at the possible origins of the LAPSs.

6.1. Crater filling as a possible origin of LAPSs

The arched shape of the LAPSs naturally suggests a possible link with craters. Some of the circular objects on UL are obviously buried craters that lay either on buried layered deposits (paleo-surface) or on the bedrock. Subsequent accumulation of deposits of ice on these irregularities would lead to an increasingly smooth surface topography that would nevertheless conserve a spatial signature of the initial formations with a decreasing vertical relief. In particular, the common hillocks observed along the crests could be easily interpreted in terms of crater rim prominences. However, the observed LAPSs are just semi-circular with no sign of an opposite and symmetric formation to complete the circle. Nevertheless, it should be possible to fill a particular crater or bedrock formation with successive deposits of layers in order to obtain a LAPS morphology. One possibility would be to start with a crater that has been asymmetrically eroded. Uneven deposition of ice on a crater is another mechanism that could produce a LAPS by accumulation of the deposits preferentially on one side. However, even if a LAPS production process based on crater filling can be imagined, it does not easily explain the spatial repetitions that are observed (Howard, 2000). The repetition and similar dimensions of the LAPSs as well as their local layout in aligned formations does not support craters as the origin given that crater locations and diameters are basically random.

6.2. Erosion processes as a possible origin of LAPSs

Howard (2000) performed a complete survey of optical images in order to detect surface signatures of eolian processes over the PLDs. He noticed similarities between the arched shape of LAPSs and barchan dunes formed by deposition of wind-transported sand. Since this study, the availability of an accurate digital elevation model (MOLA) allows us to show that LAPSs are instead deep depressions in the ice. This raises the possibility of LAPS formation by erosion of the ice, which could be driven either by eolian processes or sun sublimation.

The long-term efficiency of the wind loaded with abrasive particles to shape the surface of the ice is well known (e.g. Howard, 2000; Koutnik et al., 2005). Wire brush terrains, snakes, and trailing grooves are especially common eolian formations encountered on Planum Australe. They extend for hundreds of kilometers and are associated with a decameter vertical scale (Koutnik et al., 2005). The objects thus formed have a vertical / horizontal ratio several orders of magnitude smaller than the typical dimensions of LAPSs. However, the relatively uniform orientation of the LAPSs is consistent with an eolian origin, except for the quasi-perpendicular LAPSs found in a single region as shown in Fig 2.

At the North Pole, Planum Boreum exhibits numerous spiral troughs in its margin. Their asymmetric cross-sections are quite similar to those of the LAPSs. Although their precise origin is not yet well understood, northern troughs are thought to be sustained by a process involving solar sublimation of the exposed slope together with deposition of water vapor on the pole-facing slope, leading to an asymmetric outcrop (e.g. Pelletier, 2004 and references therein). Ice flow and katabic winds could also play a key role in their evolution (Fisher et al., 2002; Smith et al., 2010). In particular, Smith et al. (2010) suggest trough migration to explain the asymmetric stratigraphy of the troughs. They suggest that katabatic winds remove material from the upwind slopes of a trough and carry it to the downwind slope. However, northern troughs have linear shapes up to

hundreds of kilometers long, roughly arranged in a spiral leading out from the pole all around the cap, while LAPSs are individually restricted to a 20-km arch shape in the heart of a single region of Planum Australe. In addition, the hillocks often observed along the crests of the LAPS are not observed on the northern troughs. Thus, spatial shape and distribution considerations do not contribute to a common origin of the northern and southern scarps. Furthermore, LAPS orientations are not preferentially sunward and a number of them have their straight slope with outcrops almost parallel to longitudes, meaning that sun sublimation is not likely to have initiated them.

6.3. Tectonic scenario

On Earth, a common mode of crustal extension consists in the development of listric normal fault and their associated rollover anticline. Because of their crucial importance for commercial prospecting (hydrocarbon traps in faulted/folded strata), these structures have been studied extensively (e.g. Dula, 1991; Poblet and Bulnes, 2005; Shelton, 1984).

Listric faults can be defined as curved normal faults in which the fault surface is concave upwards, its dip angle decreasing with depth. These faults occur in extension zones where there is a main detachment fracture following a curved path that connects to a horizontal décollement.

The hanging-wall may develop a syn-tectonic rollover anticline classically interpreted as a direct consequence of layer bending during hanging-wall displacement above the listric normal fault (Fig. 9). The rollover geometry is conventionally interpreted as a direct consequence of the gradual bending of the strata of the hanging-wall moving along the listric normal fault. The shift changes with a horizontal component that increases with depth to become parallel to the

347 décollement. It is generally accepted that the latter is a level where fluid pressure is abnormally
348 high or where materials are weak.
349 The morphology of the LAPSs observed on Mars is very similar to the above listric fault
350 formation on Earth. They show a topographic asymmetry with a steeply dipping scarp facing a
351 gentle flexure that flattens with elevation, producing a convex morphology. The radargram
352 cross-section confirms this similarity by revealing the subsurface layer geometry. The similarity
353 with a terrestrial example is striking (see Fig. 10). The footwall compartment clearly shows
354 horizontal layers that appear to intersect with the escarpment, while the hanging-wall shows a
355 flexural geometry with a gradual downward bending of layers toward the scarp.
356
357 * Location of Fig. 9 (1 column width).
358 * Location of Fig. 10 (1 column width).
359
360 The LAPS morphology on Mars thus appears to correspond to the formations produced around a
361 listric normal fault on earth. The length of the scarp may correspond to the fault slip. The fault
362 has a strong dip angle with respect to the outcrop, which decreases with depth to reach a level
363 that may be the ice/bedrock interface.
364 Figure 9C shows a more complex evolution of the system with some subsequent faulting and
365 tilting of individual blocks (Davison, 1986; Hauge and Gray, 1996; Song and Cawood, 2001;
366 Williams and Vann, 1987). It is similar to the surface characteristics observed on cross-sections
367 4a-4a' and 4b-4b'. The presence of this rollover geometry suggests extensive regional tectonic
368 activity related to the slow sliding of Planum Australe on a geological time scale. In some
369 particular situations, the semi-circular topographic scarp may correspond to some pre-existing
370 impact crater rims associated with a circular and normal faulting system. Such structural systems

371 favor the preferential sliding of the UL polar layered region. The implied horizontal displacement
372 would be substantial (several kilometers, depending on the LAPS length) and mainly directed
373 toward the quadrant of the circular histogram Fig. 3.
374 The rollover hypothesis can be tested by modeling the tectonic process, for instance using the
375 area balance technique conventionally used for the restoration of a balanced cross-section
376 (Davison, 1986; Faure and Seguret, 1988; Gibbs, 1983). The principle is based on the concept of
377 plane strain or volume conservation of cross-sectional area. In Fig. 9B, it consists in measuring
378 the area below the regional datum (area A) which is, in the case of volume conservation, equal to
379 the volume displaced (area B). The latter is the product of the horizontal extension and the depth
380 of the décollement ($A = B = h \times d$). In such a model, it is assumed that the hanging-wall deforms
381 by simple shear and that the footwall remains undeformed throughout the extension (White et al.,
382 1986). The horizontal displacement (H_r in Fig. 11) can be directly inferred from the cross-
383 sections (if the latter is parallel to the tectonic strike). Indeed, in the case of a listric fault, the
384 deformation of the hanging-wall must be similar to simple shear deformation. Most of the shear
385 angles used for earth materials are around 60° (Dula, 1991). Compensation to 60° of potential
386 gap implies that the cutoff point of the hanging-wall is projected at 60° with respect to the surface
387 of the listric fault (Fig. 11). The horizontal displacement can be calculated as:
388 $H_r = H_a + h_v/tg(60°)$. In some case, due to slight curvature, the cutoff point may be difficult to
389 locate. We chose to use a range of possibilities between a minimum position and a maximum
390 position (Fig. 11). Thus, we can deduce a range for the depth of the décollement level which can
391 be compared to the range of the ice/bedrock interface depth inferred by MARSIS.
392
393 * Location of Fig. 11 (1 column width).

Using the geometric and topographic data, we built various LAPS models. Table 1 and associated Fig. 12 gives the results of the 8 profiles tested. For each profile, we calculated the minimum, maximum and average values of the décollement level vs depth of the bedrock interface. From Fig. 12, it appears that the depths of the décollement levels, deduced from the above models, are in good agreement with the regional depths of the bedrock interface, except for profiles 3a-3a' and 4b-4b'. For these last profiles, the depth of décollement is overestimated or underestimated by about 1 km compared to the depth of the bedrock. Of course, these disagreements could be produce by local singularities of the bedrock topography that cannot be detected by Marsis. A byproduct of this test is the horizontal displacement H_r. It appears that the listric fault scenario agrees with a substantial (4-5 km on the average) horizontal displacement of the ice, corresponding approximately to 0.5 to 1% of the UL width. These values are consistent with those usually encountered for terrestrial rollover analogs. For instance, the seismic profile presented in Fig. 10 corresponds to a horizontal displacement of about 10 km (Zhang, 1994).

* Location of Table 1.

* Location of Fig. 12 (1 column width).

7. Discussion and conclusions

We have provided a complete description of particular polar scarps observed in the ice of UL, a large outlying region of Planum Australe. Cross-analyses of topographic data, optical images, and subsurface radar observations were used to derive a morphologic and stratigraphic scheme for

these scarps that we refer to as LAPS (Large asymmetric polar scarps) because of their particular cross-section with a trough between a straight and a convex upward slope, along with outcrops on the straight slope only. Although the scarps have a weak slope, they commonly reach more than half the thickness of the PLD made up of 1 to 1.5 km of stacked ice. The LAPSs are numerous and widespread over UL, but they all have similar dimensions.

Surface features on Martian PLDs are usually explained in terms of depositional and/or erosion processes. (e.g. Fisher et al., 2002; Howard, 2000; Koutnik et al., 2005; Smith and Holt, 2010). As an alternative process, we suggest a mechanical failure of the ice for the LAPSs origin, based on their striking similarities in shape and size with rollover anticlines above listric normal faults. A quantitative model, based on area balance technique, has been briefly introduced to roughly test this hypothesis by computing some dimensions of a few basic geometries (Davison, 1986; Faure and Seguret, 1988; Gibbs, 1983). It appears that the expected depth of the décollement agrees with the bedrock depth inferred by Marsis for most of the LAPSs. It would be of interest to extend this method in the future to all the LAPSs. This system is also associated with horizontal displacement, computed to be 4-5 km on average for the LAPSs. This result agrees with what is usually observed for terrestrial rollover analogs, and would imply a substantial global outward sliding of the PLD. Such sliding has already been suggested by Murray et al. (2001) based on fractures observed along with undeformed layers outcropping from Planum Australe margins. Such peripheral fractures could be damping structures resulting from an outward sliding from the heart of UL. The sliding of an ice sheet is a process requiring a weak basal shear stress. Such conditions could be met in case of (i) incompetent basal sediments, (ii) basal sediments softened by melt-water, (iii) over-loaded salt acting as lubricant (Jackson et al., 1994), or (iv) a lower yield stress of Martian ice compared to Earth ice (Banks and Pelletier,

2008). No information is available to determine whether such sliding could occur at present day or not.

Why the PLD exhibits an outward motion is also a major question resulting from the sliding hypothesis. Possible explanations include (i) an active tectonic displacement of the underlying bedrock, (ii) a simple gravitational readjustment of the accumulated ice stack, or (iii) a fluid basal-material naturally dragged up and drained outward by the weight of the glacier.

The link between the tectonic hypothesis and the hillocks often observed along the LAPS crests remains to be determined. The hillocks are possibly related to (i) a post-deposition of icy materials, in which case the LAPS topography, under the dominant wind-stream, would generate depressions and cold traps along the crests, ~~(ii) a slight elastic rebound of the footwall after the breaking of the ice, as is commonly observed for Terrestrial tectonic phenomenon (e.g. Weissel and Karner, 1989; Westaway, 1992) and could be in our Martian case a natural consequence of listric faulting, the magnitude of which holds information on the ice rheology,~~ (ii) a rheological response to a change in basal conditions as observed around subglacial lakes on Earth (Remy et al., 1999).

A deeper study of possible tectonic activity in UL should be undertaken because of its implications on the ice rheology and PLD basal conditions. In particular, it could be a macro-expression of fundamental differences between ice-sheet behavior under Martian and Terrestrial conditions, given that the viscosity of ice on Earth would not be expected to generate such faulting.

Acknowledgements

The Shallow Radar (SHARAD) was provided by the Italian Space Agency and operated by the InfoCom Department, University of Rome ‘‘La Sapienza’’. Thales Alenia Space Italia is the prime contractor for SHARAD and is in charge of in-flight instruments and the SHARAD Operations Center. The Mars Reconnaissance Orbiter mission is managed by the Jet Propulsion Laboratory, California Institute of Technology, for the NASA Science Mission Directorate, Washington, DC. Lockheed Martin Space Systems, Denver, Colorado, is the prime contractor of the orbiter. The authors are grateful to the European space agency (ESA) and the French space agency (CNES) for supporting this work. We thank Pierre Beck, Harvey Harder and two anonymous reviewers for their careful reviews that greatly improved this paper.

488

489

490

491

492 **References**

493

494 Banks, M. E., Pelletier, J. D., 2008. Forward modeling of ice topography on Mars to infer basal
495 shear stress conditions. Journal of Geophysical Research (Planets). 113**,** 01001.
496 Byrne, S., History and current processes of the Martian polar layered deposits. California Institute
497 of Technology, Pasadena, California, 2003.
498 Clifford, S. M., 1987. Polar basal melting on Mars. Journal of Geophysical Research. 92**,** 9135-
499 9152.
500 Clifford, S. M., et al., 2000. The State and Future of Mars Polar Science and Exploration. Icarus.
501 144**,** 210-242.
502 Cutts, J. A., Lewis, B. H., 1982. Models of climate cycles recorded in Martian polar layered
503 deposits. Icarus. 50**,** 216-244.
504 Davison, I., 1986. Listric normal-faults profiles - Calculation using bed-length balance and fault
505 displacement. Journal of Structural Geology. 8**,** 209-210.
506 Dula, W. F., 1991. Geometric-models of listri normal faults and rollover folds. Aapg Bulletin-
507 American Association of Petroleum Geologists. 75**,** 1609-1625.
508 Faure, J.-L., Seguret, M., 1988. Importance des modèles de failles dans l'équilibrage des coupes
509 en distension. in L'équilibrage des couches géologiques : buts, méthodes et applications.
510 (Gratier J.P., Ed.), pp-85-92. CAES, Rennes, France. ISSN: 0755-978-X. 85-92.

511 Fisher, D. A., et al., 2002. Lineations on the "white" accumulation areas of the residual northern
512 ice cap of Mars: Their relation to the "accublation" and ice flow hypothesis. Icarus. 159**,**
513 39-52.
514 Gibbs, A. D., 1983. Balanced cross-section construction from seismic sections in areas of
515 extensional teconics. Journal of Structural Geology. 5**,** 153-160.
516 Gooding, J. L., Possible significance of cubic water-ice, H2O-Ic, in the atmospheric water cycle
517 of Mars. In: L. a. P. Institute, (Ed.), MECA Workshop on Atmospheric H2O Observations
518 of Earth and Mars. Physical Processes, Measurements and Interpretations, 1988, pp. 46-
519 49.
520 Grima, C., et al., 2009. North polar deposits of Mars: Extreme purity of the water ice.
521 Geophysical Research Letters. 36.
522 Hauge, T. A., Gray, G. G., 1996. A critique of techniques for modeling normal-fault and rollover
523 geometries. In Modern developments in structural interpretations, validation and
524 modeling.
525 Hays, J. D., et al., 1976. Variations in the Earth's Orbit: Pacemaker of the Ice Ages. Science. 194**,**
526 1121-1132.
527 Head, J. W., 2001. Mars: Evidence for geologically recent advance of the south polar cap. Journal
528 of Geophysical Research-Planets. 106**,** 10075-10085.
529 Head, J. W., et al., 2003. Recent ice ages on Mars. Nature. 426**,** 797-802.
530 Head, J. W., Pratt, S., 2001. Extensive Hesperian-aged south polar ice sheet on Mars: Evidence
531 for massive melting and retreat, and lateral flow and pending of meltwater. Journal of
532 Geophysical Research-Planets. 106**,** 12275-12299.
533 Herkenhoff, K. E., Plaut, J. J., 2000. Surface Ages and Resurfacing Rates of the Polar Layered
534 Deposits on Mars. Icarus. 144**,** 243-253.

535 Howard, A. D., 2000. The role of eolian processes in forming surface features of the Martian
536 polar layered deposits. Icarus. 144**,** 267-288.
537 Jackson, M. P. A., et al., 1994. STRUCTURAL DYNAMICS OF SALT SYSTEMS. Annual
538 Review of Earth and Planetary Sciences. 22**,** 93-117.
539 Jaumann, R., et al., 2007. The high-resolution stereo camera (HRSC) experiment on Mars
540 Express: Instrument aspects and experiment conduct from interplanetary cruise through
541 the nominal mission. Planetary and Space Science. 55**,** 928-952.
542 Kargel, J. S., Strom, R. G., 1992. Ancient glaciation on Mars. Geology. 20**,** 3-7.
543 Kolb, E. J., Tanaka, K. L., 2001. Geologic history of the polar regions of Mars based on Mars
544 global surveyor data - II. Amazonian period. Icarus. 154**,** 22-39.
545 Koutnik, M., et al., 2002. South Polar Layered Deposits of Mars: The cratering record. Journal of
546 Geophysical Research-Planets. 107.
547 Koutnik, M. R., et al., 2005. Eolian controlled modification of the martian south polar layered
548 deposits. Icarus. 174**,** 490-501.
549 Laskar, J., et al., 2002. Orbital forcing of the martian polar layered deposits. Nature. 419**,** 375-
550 377.
551 Lewis, S. R., et al., 1999. A climate database for Mars. Journal of Geophysical Research-Planets.
552 104**,** 24177-24194.
553 McEwen, A. S., et al., 2007. Mars Reconnaissance Orbiter's High Resolution Imaging Science
554 Experiment (HiRISE). Journal of Geophysical Research-Planets. 112**,** 40.
555 McGovern, P. J., et al., 2004. Localized gravity/topography admittance and correlation spectra on
556 Mars: Implications for regional and global evolution (vol 107, pg 5136, 2002). Journal of
557 Geophysical Research-Planets. 109**,** 5.

558 Milkovich, S. M., et al., 2002. Meltback of Hesperian-aged ice-rich deposits near the south pole
559 of Mars: Evidence for drainage channels and lakes. Journal of Geophysical Research-
560 Planets. 107.
561 Murray, B., et al., 2001. Preliminary geological assessment of the northern edge of ultimi lobe,
562 Mars south polar layered deposits. Icarus. 154**,** 80-97.
563 Nimmo, F., Stevenson, D. J., 2000. Influence of early plate tectonics on the thermal evolution and
564 magnetic field of Mars. Journal of Geophysical Research-Planets. 105**,** 11969-11979.
565 Nouvel, J. F., et al., 2004. Radar signal simulation: Surface modeling with the Facet Method.
566 Radio Science. 39**,** 17.
567 Pelletier, J. D., 2004. How do spiral troughs form on Mars? Geology. 32**,** 365-367.
568 Picardi, G., et al., 2005. Radar soundings of the subsurface of Mars. Science. 310**,** 1925-1928.
569 Plaut, J. J., et al., 2007. Subsurface Radar Sounding of the South Polar Layered Deposits of Mars.
570 Science. 316**,** 92-96.
571 Poblet, J., Bulnes, M., 2005. Fault-slip, bed-length and area variations in experimental rollover
572 anticlines over listric normal faults: influence in extension and depth to detachment
573 estimations. Tectonophysics. 396**,** 97-117.
574 Pollack, H. N., et al., 1993. Heat flow from the earths interior - Analysis of the global data set.
575 Reviews of Geophysics. 31**,** 267-280.
576 Reese, C. C., et al., 1998. Heat transport efficiency for stagnant lid convection with dislocation
577 viscosity: Application to Mars and Venus. Journal of Geophysical Research-Planets. 103**,**
578 13643-13657.
579 Remy, F. D., et al., 1999. Ice flow physical processes derived from the ERS-1 high-resolution
580 map of the Antarctica and Greenland ice sheets. Geophysical Journal International. 139**,**
581 645-656.

582 Renno, N. O., et al., 2009. Possible physical and thermodynamical evidence for liquid water at
583 the Phoenix landing site. Journal of Geophysical Research-Planets. 114.
584 Rognon, P., et al., 2007. The northern ice cap of Mars: an enigmatic evolution compared to the
585 polar environment on Earth. Bulletin De La Societe Geologique De France. 178**,** 427-436.
586 Seu, R., et al., 2004. SHARAD: The MRO 2005 shallow radar. Planetary and Space Science. 52**,**
587 157-166.
588 Shelton, J. W., 1984. Listric normal faults - an illustrated summary. Aapg Bulletin-American
589 Association of Petroleum Geologists. 68**,** 801-815.
590 Smith, D. E., et al., 2001. Mars Orbiter Laser Altimeter: Experiment summary after the first year
591 of global mapping of Mars. Journal of Geophysical Research-Planets. 106**,** 23689-23722.
592 Smith, I. B., Holt, J. W., 2010. Onset and migration of spiral troughs on Mars revealed by orbital
593 radar. Nature. 465**,** 450-453.
594 Song, T. G., Cawood, P. A., 2001. Effects of subsidiary faults on the geometric construction of
595 listric normal fault systems. Aapg Bulletin. 85**,** 221-232.
596 Tanaka, K., Scott, D., 1987. Geologic map of the polar region of mars. USGS Miscellaneous
597 Investigations Series Map I-1802-C,.
598 Thomas, P., et al., Polar deposits of Mars. In: H. H. Kiefer, et al., Eds.), Mars. Univ. of Arizona
599 Press, Tucson, 1992, pp. 767-795.
600 Thomas, P., Weitz, C., 1989. Sand dune materials and polar layered deposits on Mars. Icarus. 81**,**
601 185-215.
602 Ward, W. R., Long-term orbital and spin dynamics of mars. In: H. H. Kiefer, et al., Eds.), Mars.
603 Univ. of Arizona Press, Tucson, 1992, pp. 298-320.
604 Weidich, A., Satellite images atlas of glaciers of the world: Greenland. U. S. Geological Survey
605 Professional Paper 1386-C, p.C3, 1995.

606 Weissel, J. K., Karner, G. D., 1989. Flexural uplift of the rift flanks due to mechanical unloading
607 of the lithosphere during extension. Journal of Geophysical Research-Solid Earth and
608 Planets. 94**,** 13919-13950.
609 Westaway, R., 1992. Analysis of tilting near normal faults using calculus of variations -
610 implications for upper crustal stress and rheology. Journal of Structural Geology. 14**,** 857-
611 871.
612 White, N., et al., 1986. The relationships between the geometry of normal faults and that of the
613 sedimentary layers in their hanging walls. Journal of Structural Geology. 8**,** 897-909.
614 Williams, G., Vann, I., 1987. The geometry of listric normal faults and deformation in their
615 hangin walls. Journal of Structural Geology. 9**,** 789-795.
616 Zhang, Y. K., 1994. Mechanics of extensional wedges and geometry of normal faults. Journal of
617 Structural Geology. 16**,** 725-732.
618
619
620
621
622
623
624
625
626
627
628
629

630

631

632

633 **Table 1.** Depth of the décollement level determined for 8 LAPS profiles.

634

Profile	Min. value (km)			Max. value (km)			Measured area (km^2)	Depth of décollement (km)			Depth of bedrock (km)		
	H_a	h_v	H_r	H_a	h_v	H_r		Min. slip	Max. slip	Mean	Min.	Max.	Mean
1aa'	2.31	0.26	2.46	3.23	0.26	3.38	3.67	1.49	1.09	1.29	0.90	1.30	1.10
1bb'	2.98	0.28	3.14	3.70	0.27	3.86	1.87	0.60	0.48	0.54	0.20	0.60	0.40
2aa'	3.00	0.43	3.25	4.10	0.45	4.36	4.37	1.35	1.00	1.17	0.70	1.11	0.91
2bb'	3.20	0.35	3.40	3.80	0.34	4.00	2.75	0.81	0.69	0.75	0.70	1.11	0.91
3aa'	2.10	0.19	2.21	3.70	0.22	3.83	2.29	1.04	0.60	0.82	1.08	1.50	1.29
3bb'	5.70	0.40	5.93	8.80	0.40	9.03	5.82	0.98	0.64	0.81	0.36	0.76	0.56
4aa'	4.40	0.58	4.74	5.90	0.57	6.23	5.33	1.12	0.86	0.99	0.65	1.05	0.85
4bb'	3.80	0.55	4.12	6.90	0.55	7.22	8.11	1.97	1.12	1.55	0.67	1.04	0.86

635

636

637

638

639

640

641

642

643

644

645

646

647

648

649

650 **Figure captions**

651

652 **Fig. 1.** Shaded topography of UL (stereographic projection with illumination from the bottom-
653 right). The white line is the Planum Australe boundary. The bottom-right insert locates UL within
654 the entire polar plateau. Five black boxes delimit the regions that are enlarged in Fig. 5.

655

656 **Fig. 2.** Arch-shaped features are indicated in bold red. The arches marked by X's are LAPSs that
657 exhibit a convex slope with a more complex topography (see section 4.2 for details). White
658 arrows indicate an example of neighboring LAPSs with strictly different orientations.

659

660 **Fig. 3.** (Top) Histogram of the LAPS azimuths. The Y-axis is the number of occurrences. A
661 concavity facing north has an azimuth equal to 0°. A concavity parallel to a longitude and facing
662 decreasing west-longitudes has an azimuth equals 90°. (Bottom) Circular histogram of the
663 relative orientation of the LAPSs in a regional context. The circle border represents 25
664 occurrences. See section 4.1 for details.

665

666 **Fig. 4.** 3D view of a LAPS (located at the lower right corner of Fig. 5A). Illumination is from the
667 upper-left. Keep in mind that the vertical scale is exaggerated by a factor of 10. The volume is 45
668 km x 40 km x 1800 m. The bottom gray area depicts the expected position of the bedrock
669 detected by MARSIS (Plaut et al., 2007), taking into account the ±200 m uncertainty. Note the
670 typical asymmetric cross-section, perpendicular to the spatial arch shape, with a straight slope

facing a convex slope. The general behavior of the polar layers deduced from the stratigraphic study was added to create a typical model of a LAPS cross-section. The outcrops on the straight slope are outlined, while the downward bending of the subsurface layers is visible below the convex slope. The question mark beneath the LAPS is a reminder that no radar data regarding the subsurface structure are available at the corresponding location (see section 4.2 for details). Hillocks are also present.

Fig. 5. Five enlargements (A-E) for the corresponding regions indicated in Fig.1. The background map is the unshaded MOLA elevation map. Contour lines are separated by 50 m. Elevation color coding and the spatial scale are the same for all boxes. The black lines locate the cross-sections shown in Fig. 6. The three white rectangles delimit the extent of the images corresponding to the cross-sections in Fig. 7. An example of merging craters that were not taken into account for LAPS counting can be seen at the bottom left of box B (see section 4.1 for details).

Fig. 6. Cross-sections of some LAPSs. The cross-section locations are indicated in Fig. 5. Black lines are the surface and gray areas depict the expected position of the bedrock as retrieved from the interpolated MARSIS map (Plaut et al., 2007), taking into account the 200 m uncertainty. Elevations are indicated in meters, while horizontal lengths are in kilometers. Black arrows show hillocks when present (see section 4.3 for details). Each cross-section is represented by two profiles: (Bottom) Vertical scale multiplied by 10 to highlight the surface shape, (Top) No exaggeration of vertical scale to emphasize the relative flatness and thinness of the system.

Fig. 7. Cross-sections (5-5’ and 6-6’) of two LAPSs, associated with HRSC pictures (DLR/FU Berlin/ESA) and SHARAD radargrams (NASA/ASI). Illumination is from the left. See Fig. 5 for

695 locations. The first radargram from the top has its vertical scale multiplied by 10.The last two
696 have a vertical scale multiplied by 30 to emphasize the subsurface echoes. The colored lines in
697 the bottom radargram highlight the behavior of detected subsurface layers. The blue lines are
698 polar layered deposits and the red lines are the putative bedrock deduced by correlation between
699 the SHARAD radargram and the MARSIS basal topography. Black arrows indicate strong echoes
700 that are clutters generated by off-nadir surface reflections.
701
702 **Fig. 8.** Cross-section (7-7') of two successive LAPSs, associated with the HiRISE picture
703 PSP_06222_1055 (NASA/JPL/University of Arizona). Illumination is from the bottom-right. See
704 Fig. 5 for locations. Outcrops of layers occur only on the straight slope of the LAPSs, especially
705 clear on the LAPS on the left . For the LAPS on the right, the cross-section path cuts the end of
706 the LAPS leading to progressive fading of the outcrops.
707
708 **Fig. 9.** Sketches illustrating the typical geometric evolution of hanging-wall deformation in a
709 listric normal fault system. (A) An outward stress breaks the layered material. The dip angle of
710 the resultant fault decreases down to the level of the décollement. (B) Gradual bending of the
711 hanging-wall leads to a rollover anticline geometry. (C) Antithetic faults can follow either
712 directly steps (A) or (B) (modified from Song and Cawood (2001)).
713
714 **Fig. 10.** Seismic profile of a rollover fold associated with a listric fault in the Bohai Gulf of
715 northern China. The vertical scale is in seconds. Note that LAPSs observed on Mars are only
716 made up of pre-tectonic deposits. This rollover fold corresponds to a horizontal displacement of
717 about 10 km. 1 s is equivalent to 700 m on the vertical scale. Modified from Zhang (1994).
718

719 **Fig. 11.** Area balance for extension. *Top*: Relationship between the undeformed and deformed
720 lengths. The cutoff points are the intersection between the stratigraphic boundaries and the listric
721 fault. For a given stratigraphic horizon, we can identify a footwall cutoff point and a hanging wall
722 cutoff point. The real horizontal extension (H_r) is the sum of the apparent horizontal extension
723 (H_a) and the projected cutoff point position (H_c). *Bottom*: Because of the low curvature of the
724 listric fault and the rollover geometry, the position of the cutoff point is uncertain. Two extreme
725 positions are used giving two values of apparent horizontal extension (H_a). Uncertainty on the
726 position of the bedrock is represented by a gray band.
727
728 **Fig. 12.** Graphic illustration of the minimum, maximum and average depth of the décollement
729 level according to the minimum, maximum and average position of the bedrock for the 8 profiles
730 tested.

Figure 1

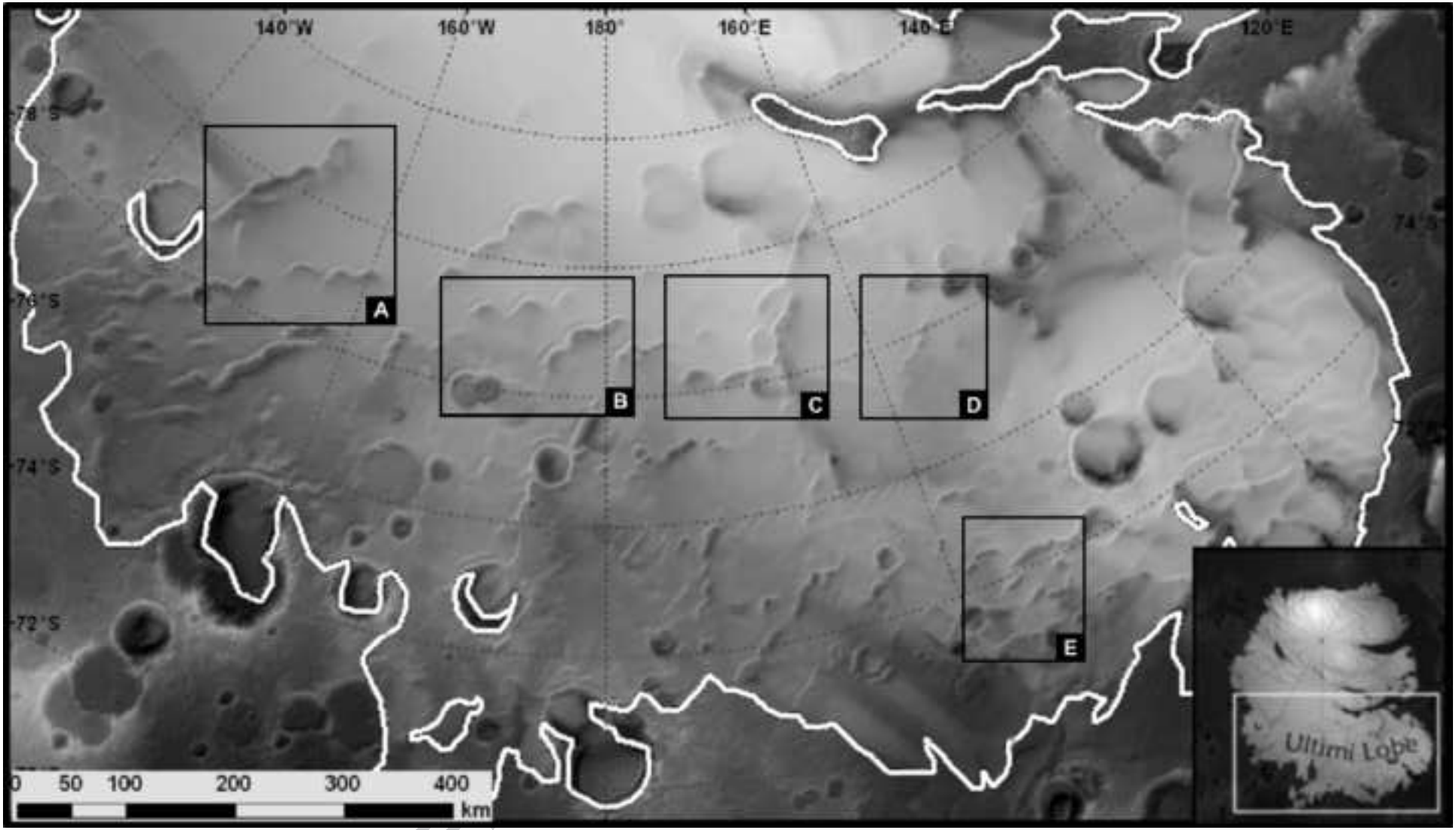

Figure 2

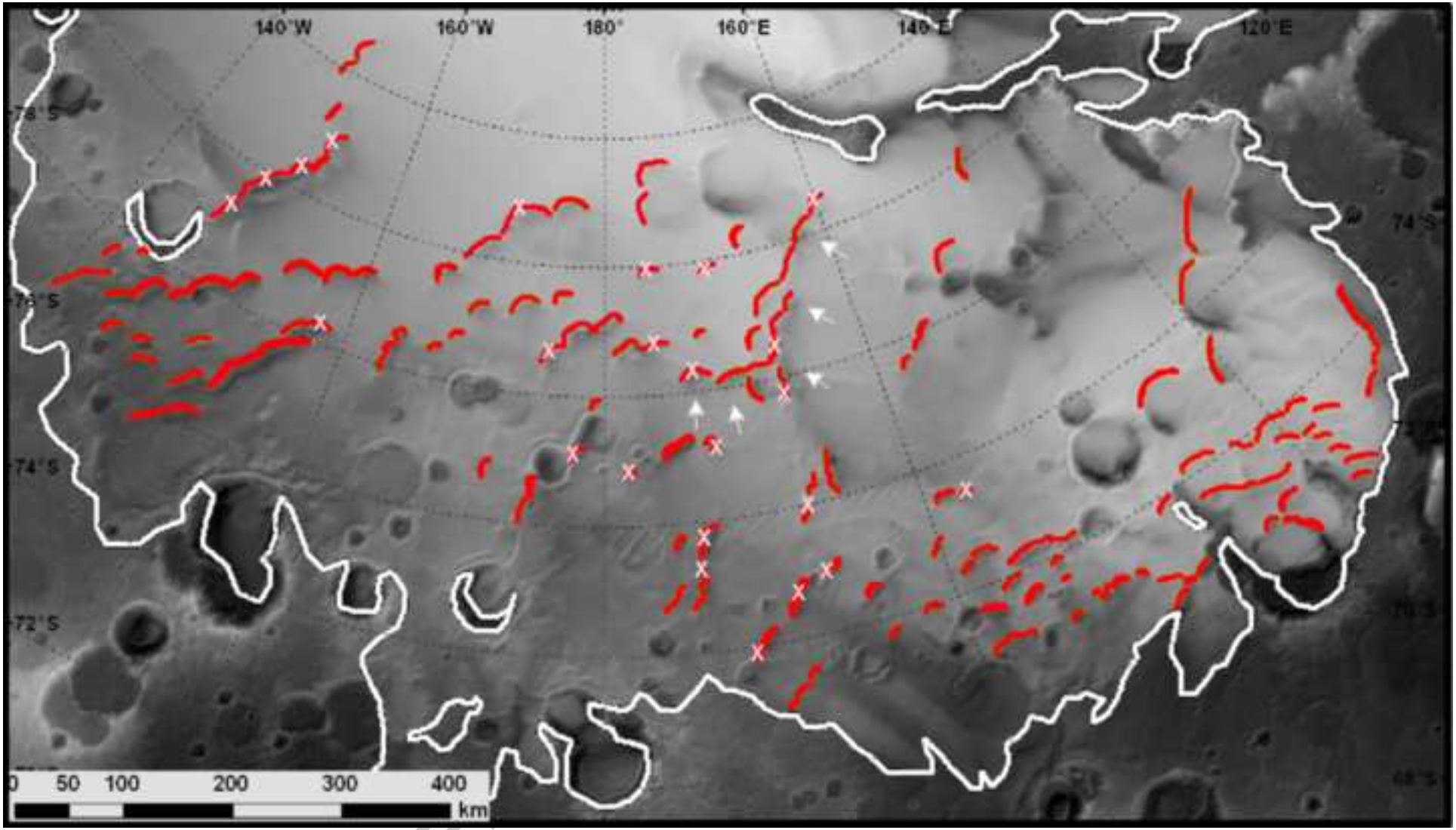

Figure 3

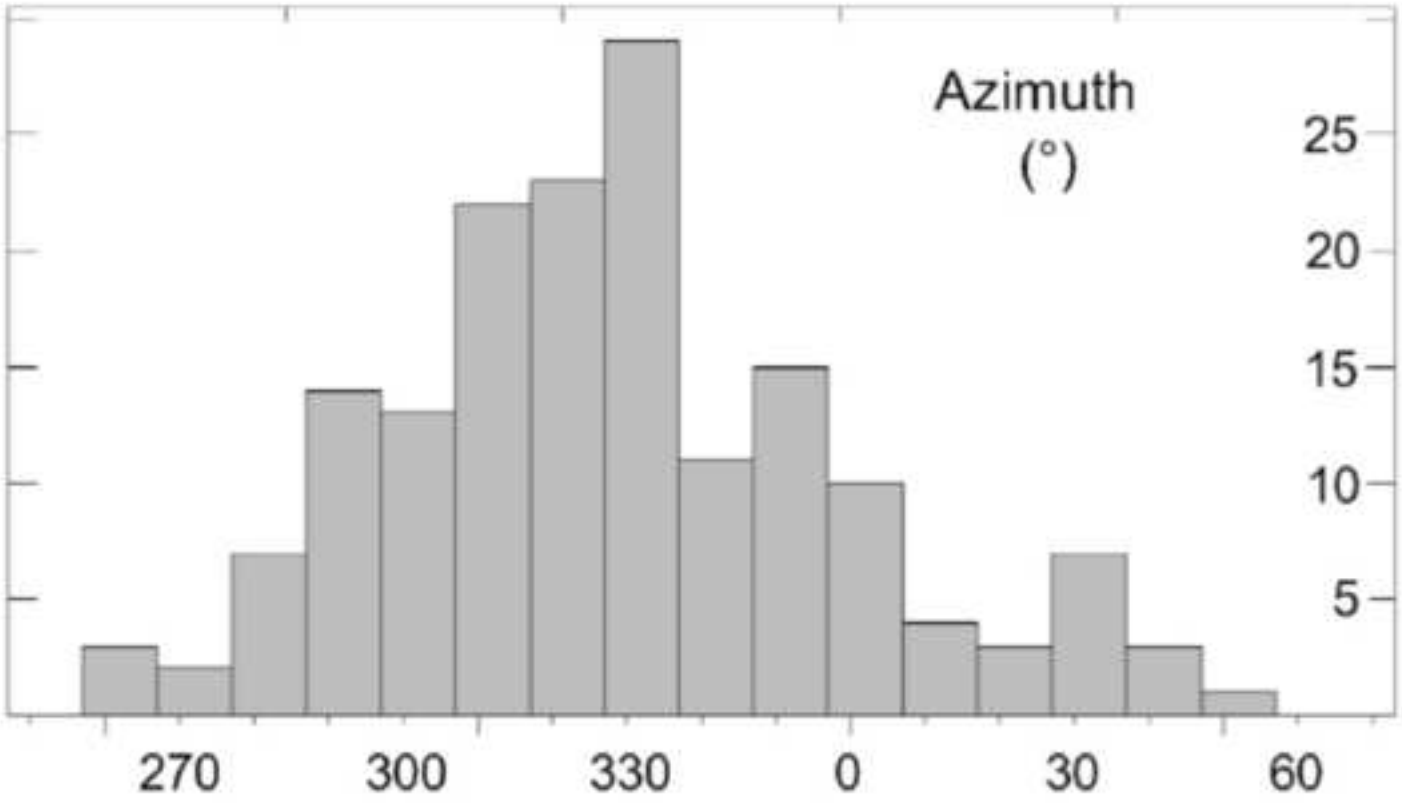

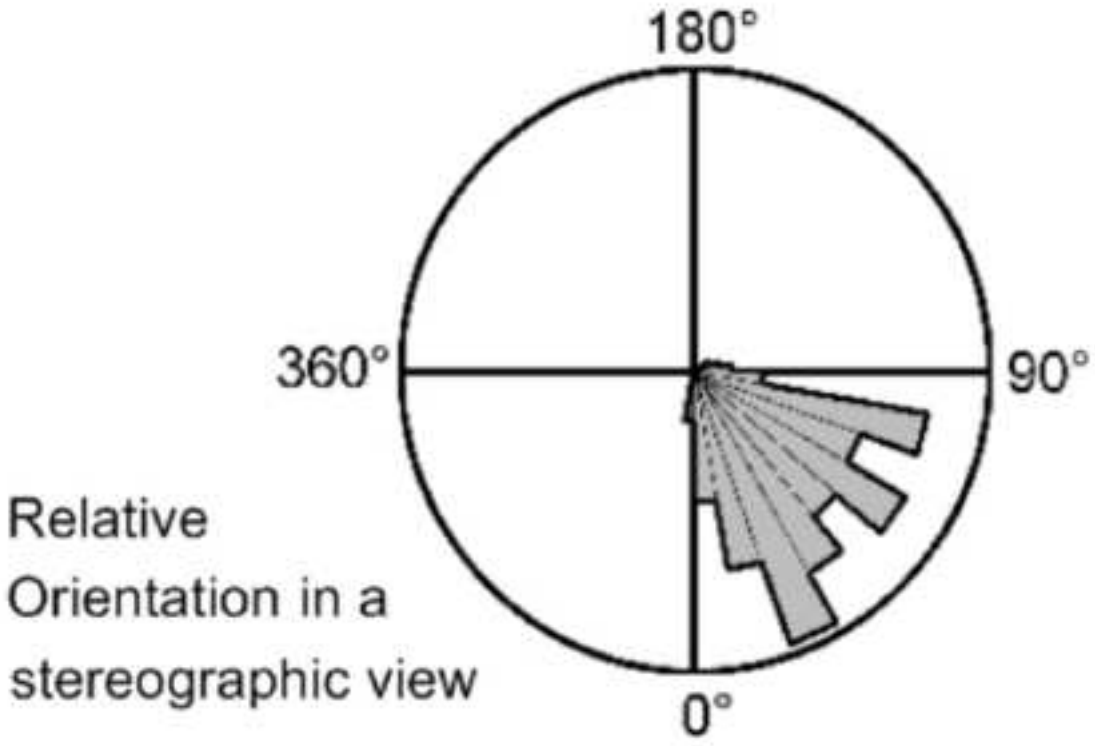

Figure 4

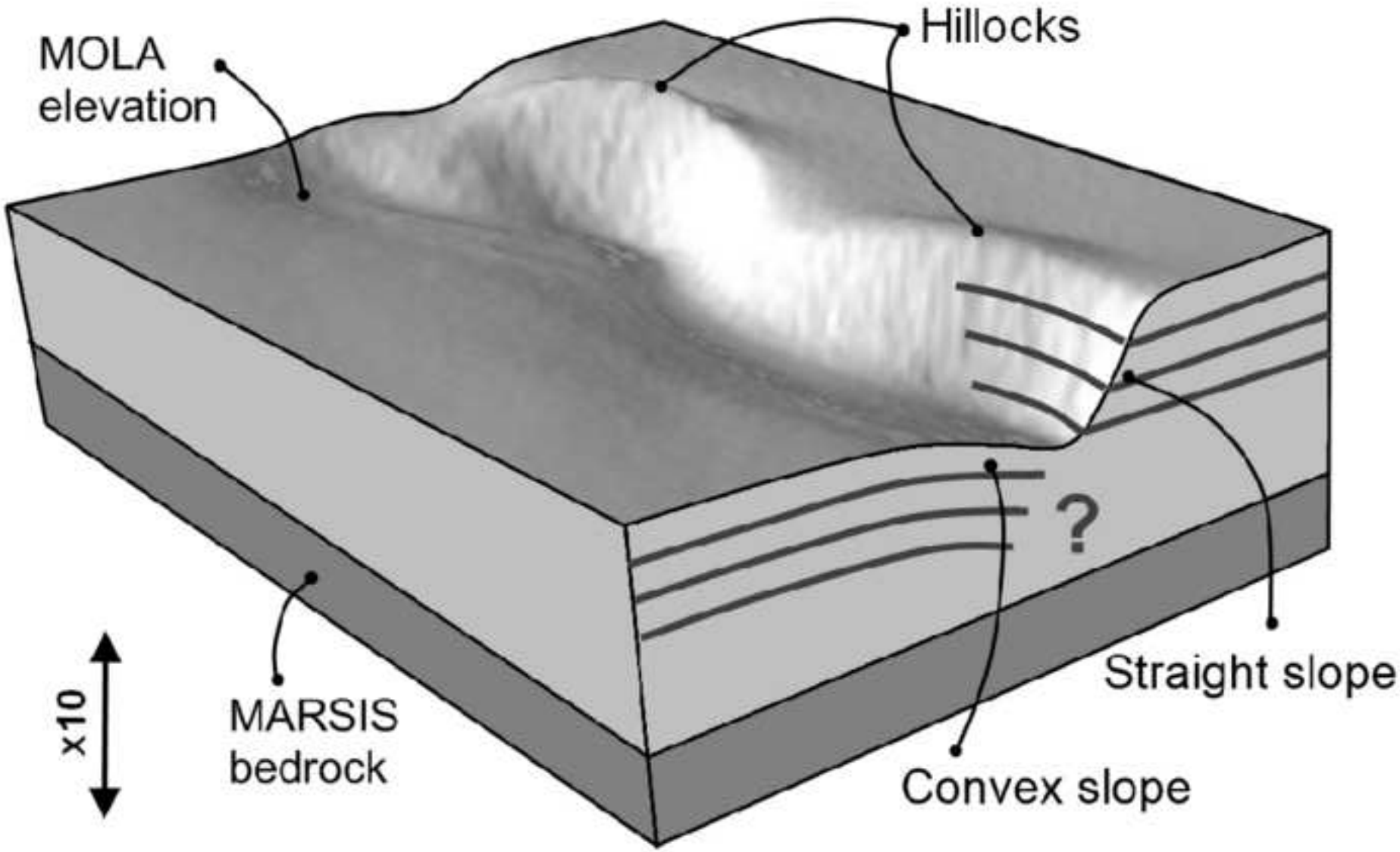

Figure 5

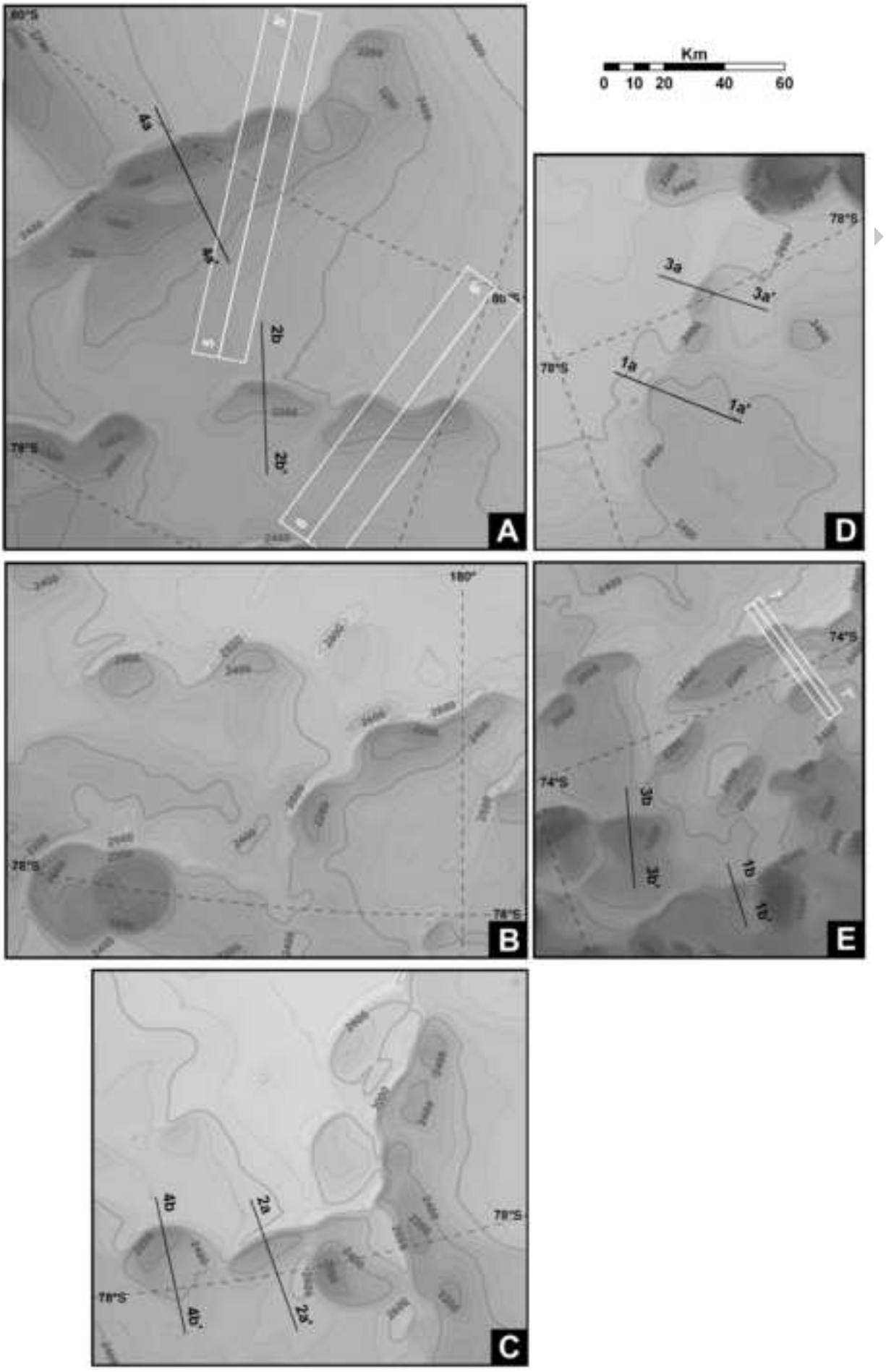

Figure 6

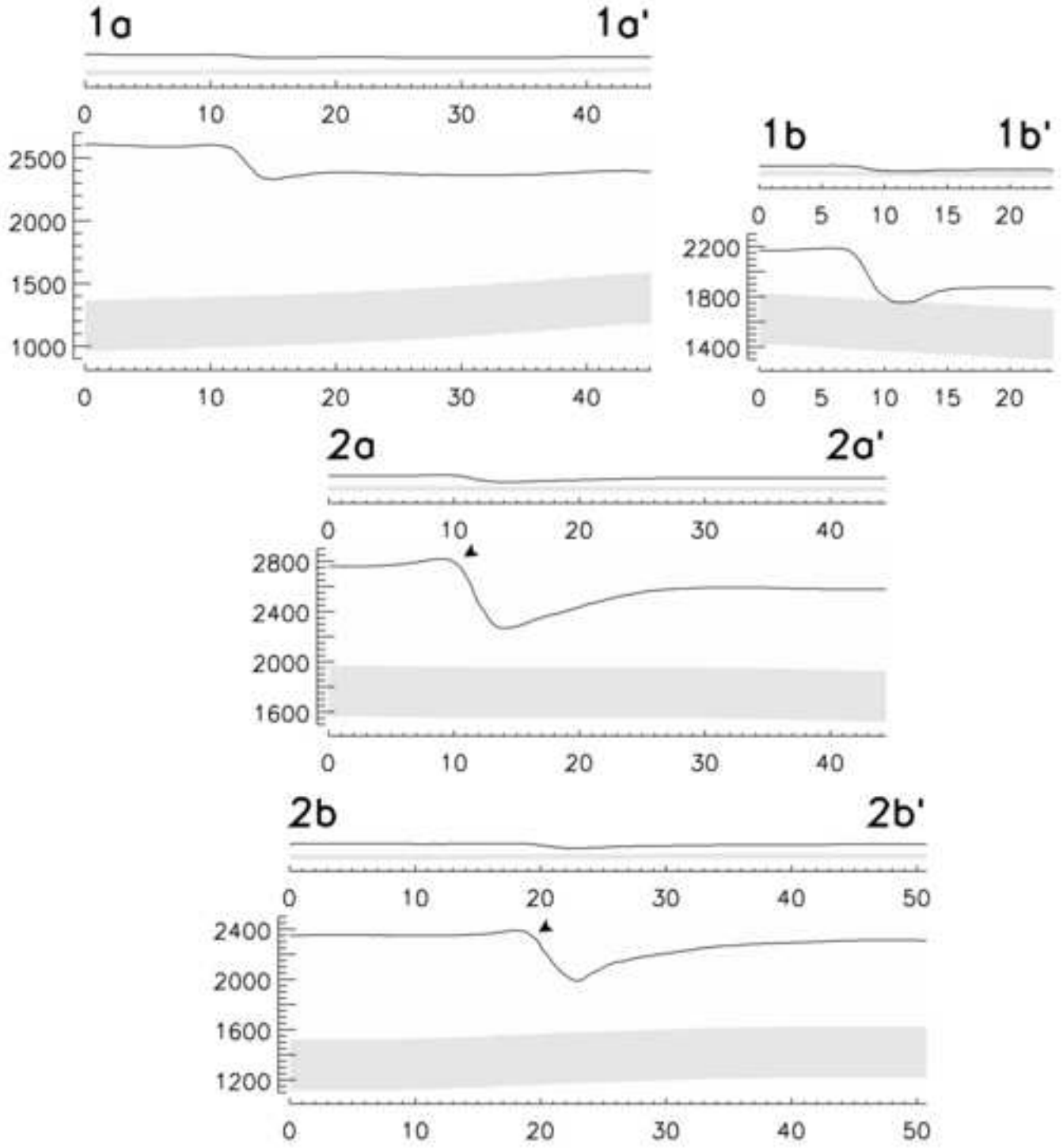

Figure 6 (continued)

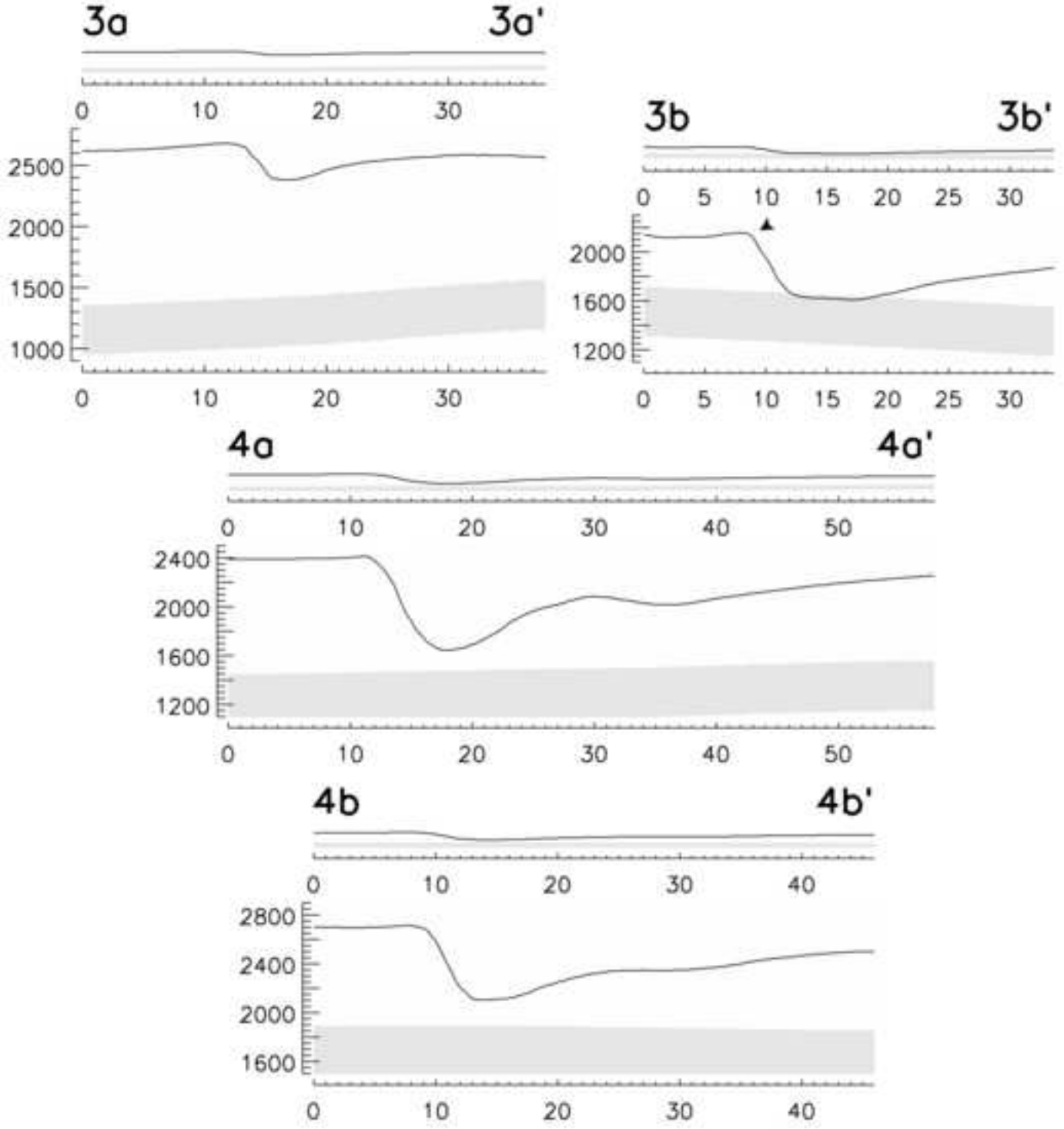

Figure 7

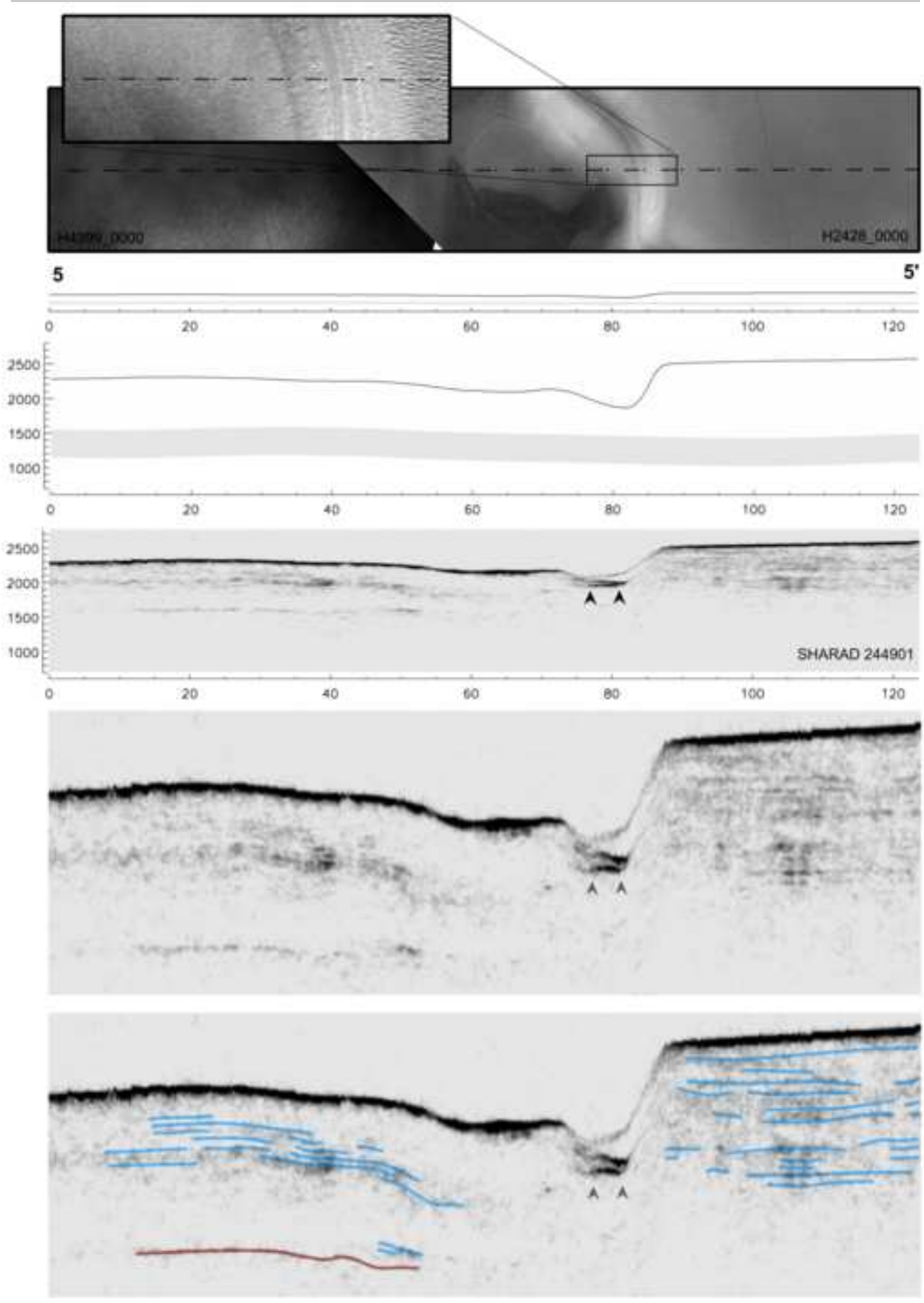

Figure 7 (continued)

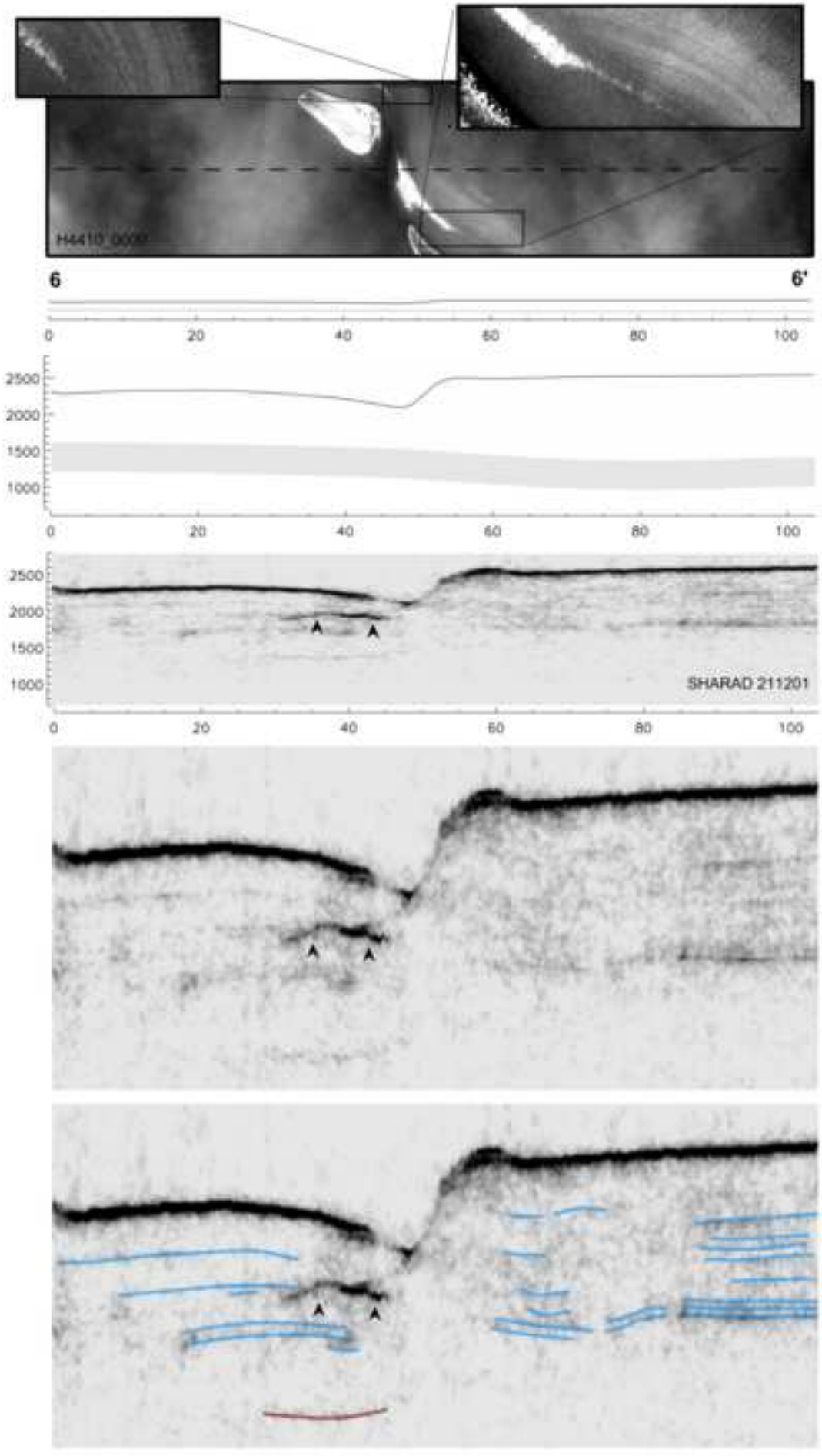

Figure 8

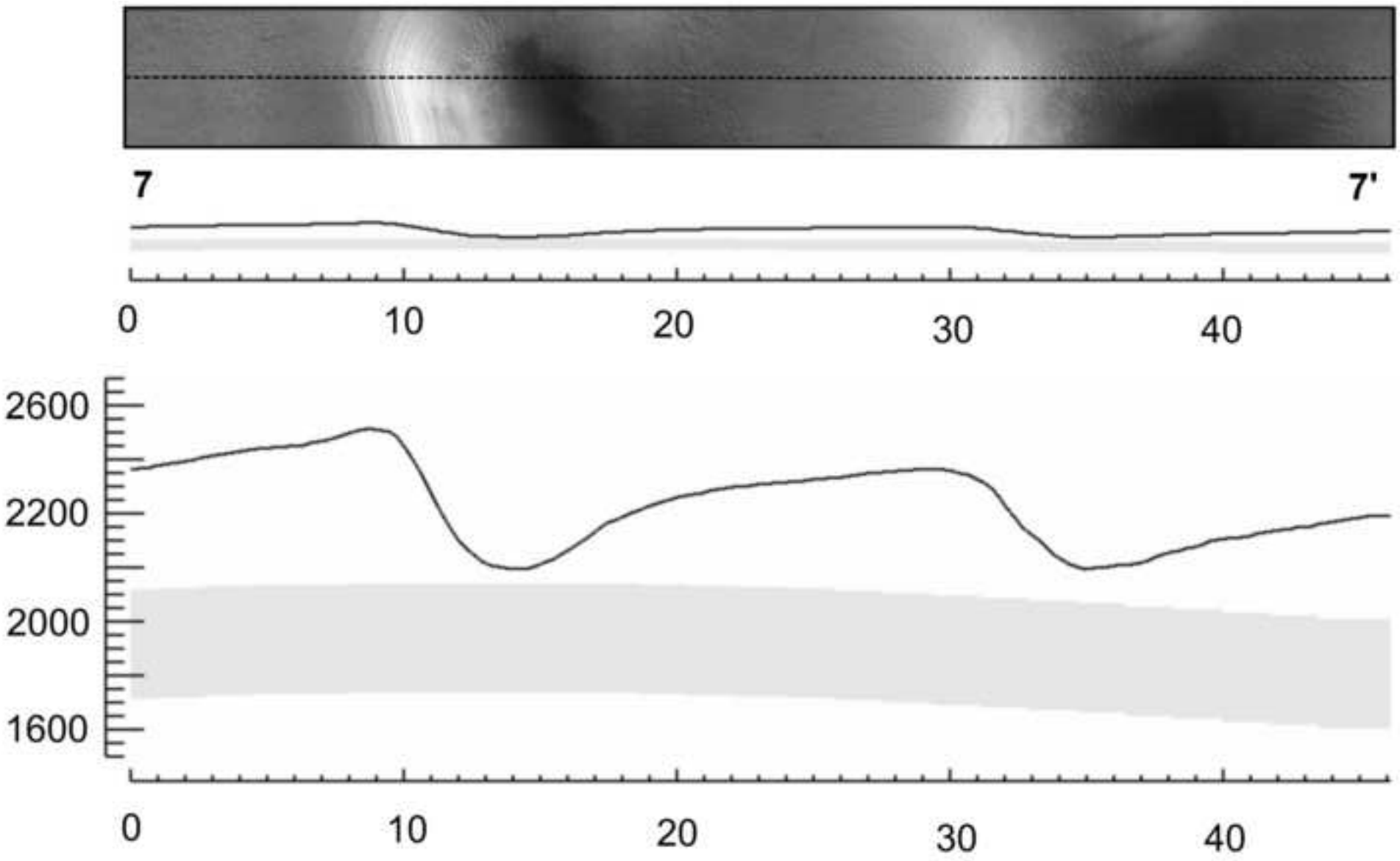

Figure 9

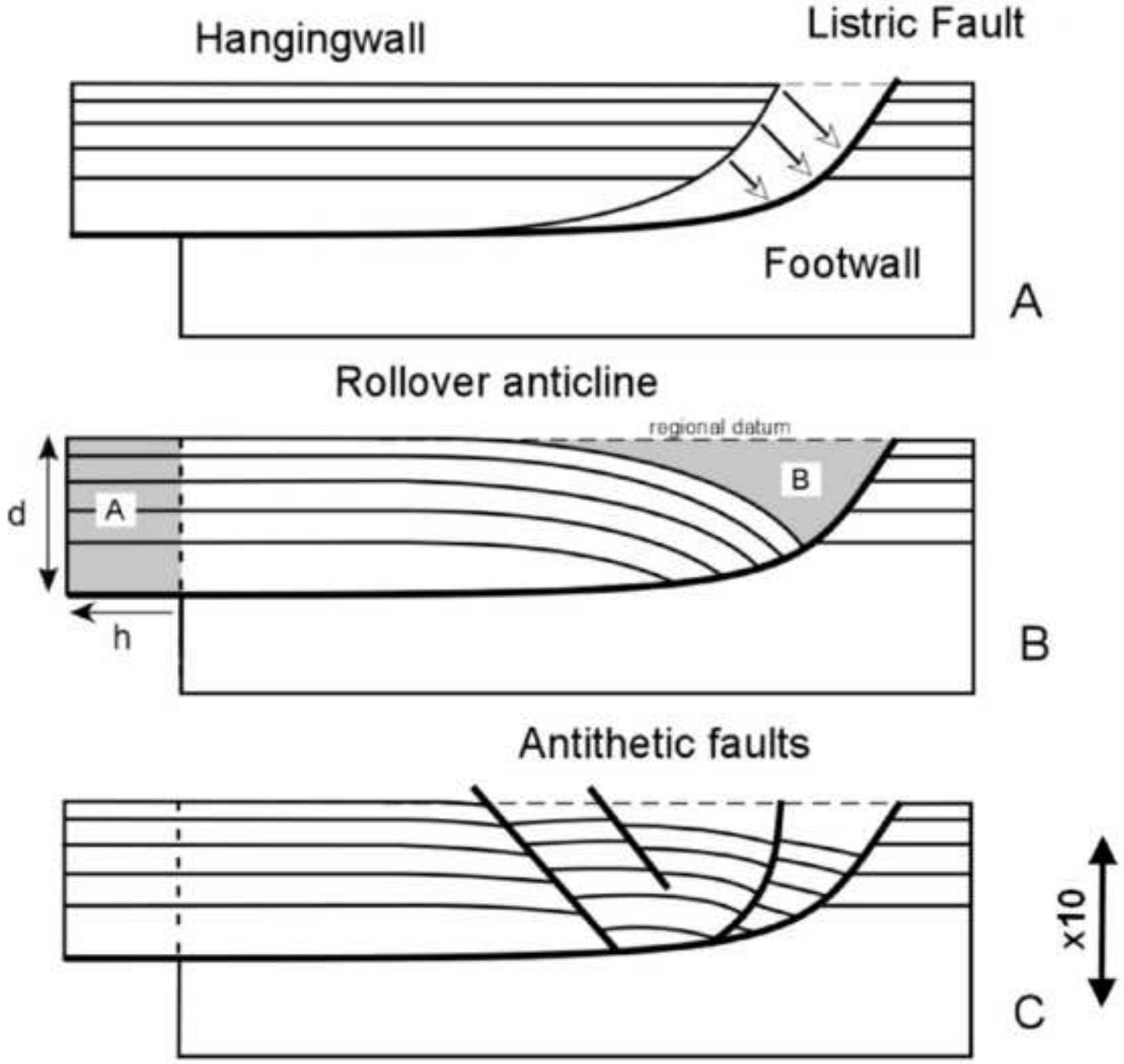

Figure 10

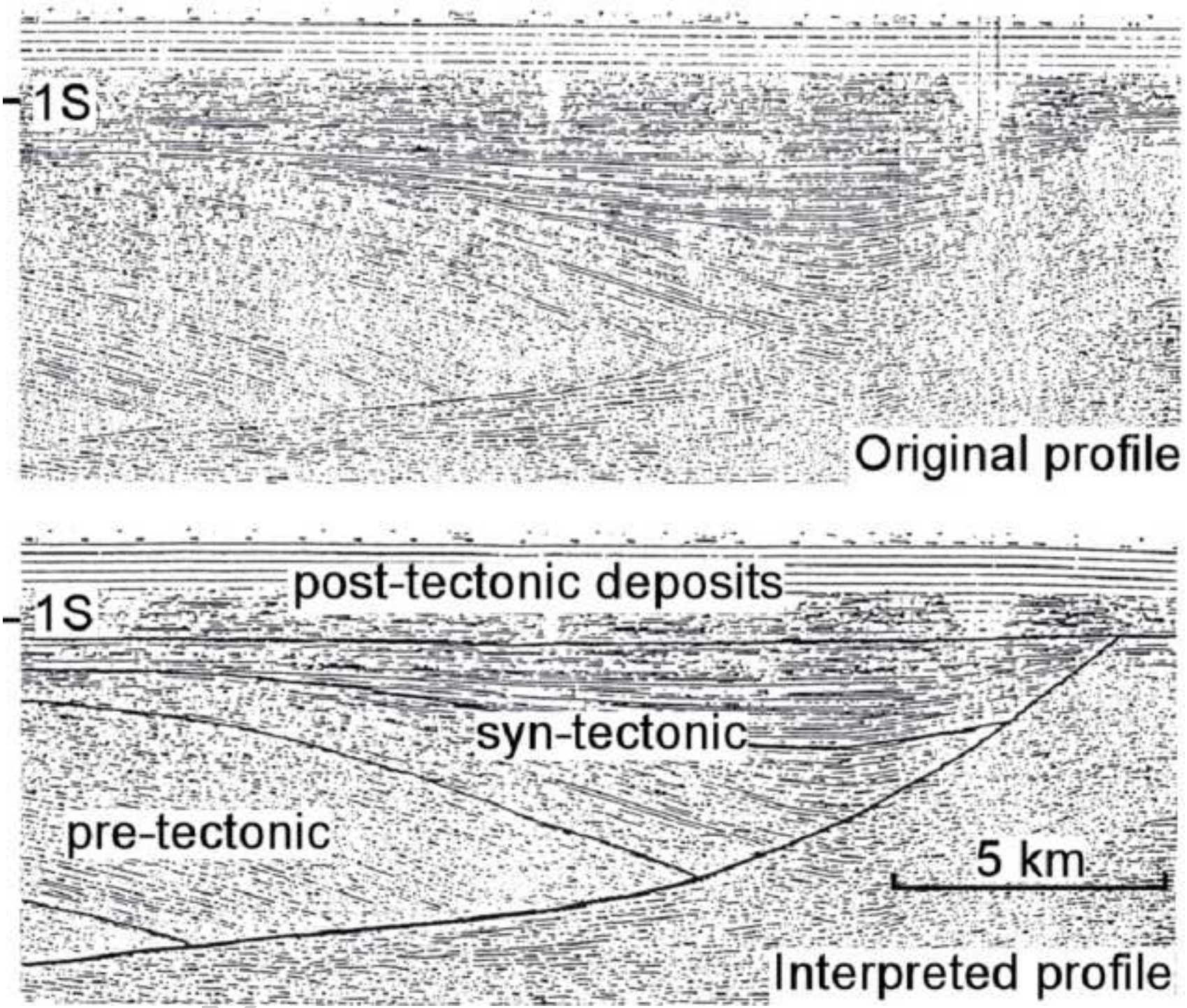

Figure 11

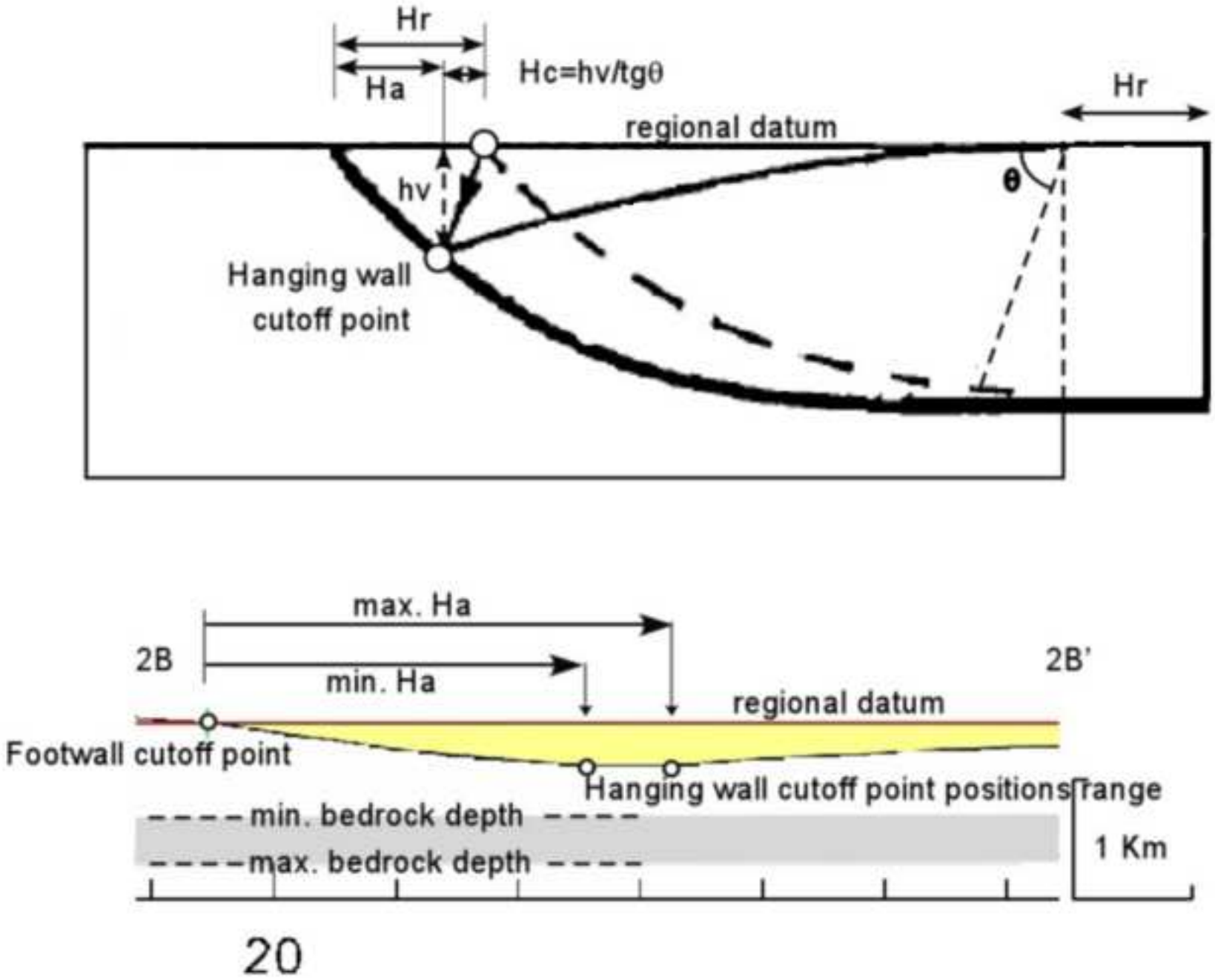

Figure 12

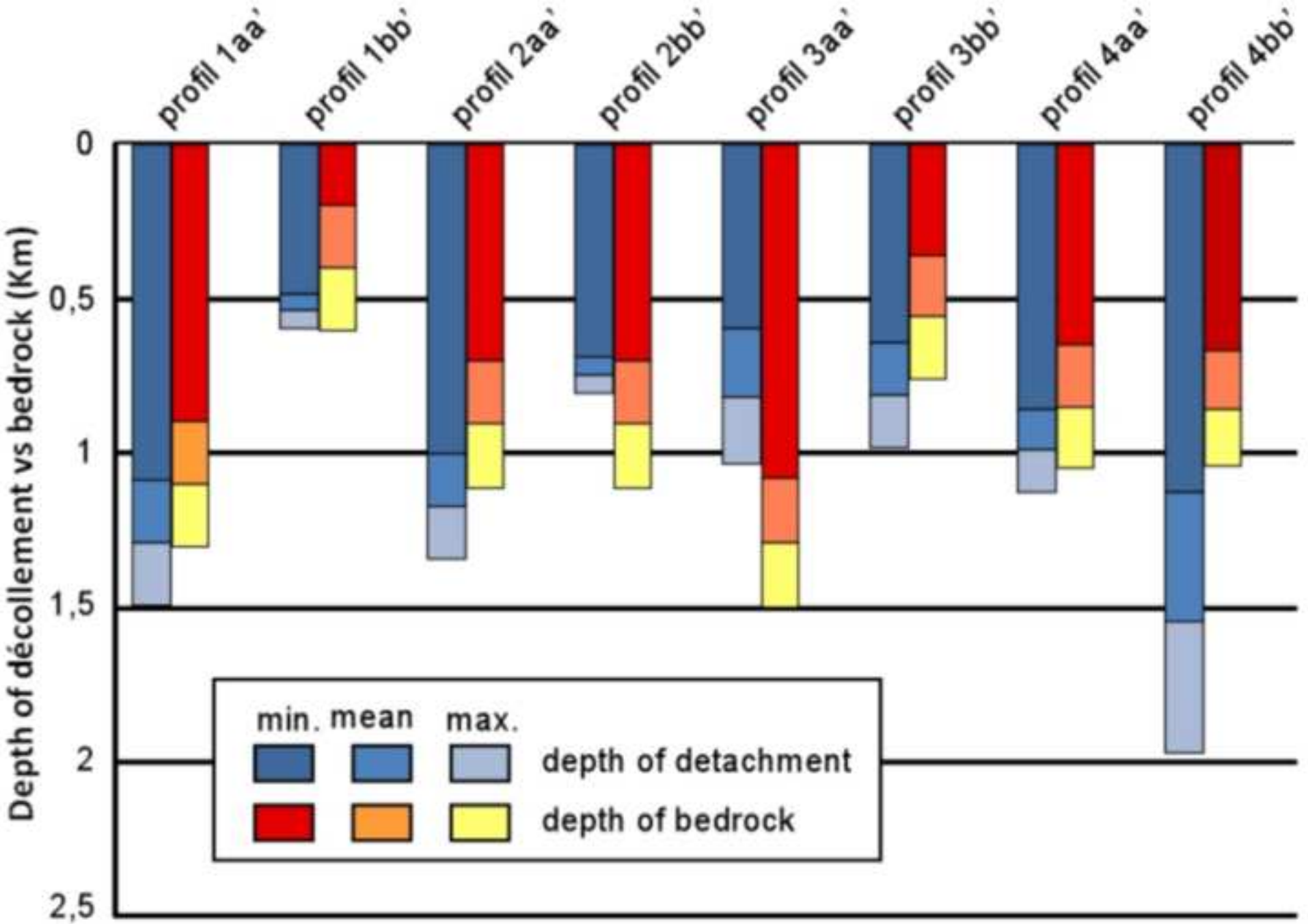

Research Highlights

- The ms makes a new and complete geomorphologic description of intriguing scarps of Planum Australe, using jointly different set of data.

- This description is similar to the cross-section of a listric normal fault. This allows proposing a new hypothesis regarding the formation process of these scarps, implying a mechanical failure of the ice and a subsequent basal sliding.

- It is emphasized that this process should be study more deeply because of its implications on the ice rheology and basal conditions